J Geod
DOI 10.1007/s00190-016-0909-6

ORIGINAL ARTICLE

Estimation of satellite antenna phase center offsets for Galileo

P. Steigenberger[1] · M. Fritsche[2] · R. Dach[3] · R. Schmid[4] · O. Montenbruck[1] · M. Uhlemann[2,5] · L. Prange[3]

Received: 8 January 2016 / Accepted: 18 April 2016

Abstract Satellite antenna phase center offsets for the Galileo In-Orbit Validation (IOV) and Full Operational Capability (FOC) satellites are estimated by two different analysis centers based on tracking data of a global GNSS network. The mean *x*- and *y*-offsets could be determined with a precision of a few centimeters. However, daily estimates of the *x*-offsets of the IOV satellites show pronounced systematic effects with a peak-to-peak amplitude of up to 70 cm that depend on the orbit model and the elevation of the Sun above the orbital plane. For the IOV *y*-offsets, no dependence on the orbit model exists but the scatter strongly depends on the elevation of the Sun above the orbital plane. In general, these systematic effects are significantly smaller for the FOC satellites. The *z*-offsets of the two analysis centers agree within the 10–15 cm level, and the time series do not show systematic effects. The application of an averaged Galileo satellite antenna model obtained from the two solutions results in a reduction of orbit day boundary discontinuities by up to one third—even if an independent software package is used.

✉ P. Steigenberger
peter.steigenberger@dlr.de

1 German Space Operations Center, Deutsches Zentrum für Luft- und Raumfahrt, Münchener Straße 20, 82234 Weßling, Germany

2 Deutsches GeoForschungsZentrum GFZ, Telegrafenberg, 14473 Potsdam, Germany

3 Astronomisches Institut, Universität Bern, Sidlerstrasse 5, 3012 Bern, Switzerland

4 Deutsches Geodätisches Forschungsinstitut, Technische Universität München, Arcisstraße 21, 80333 Munich, Germany

5 Present Address: Alberding GmbH, Schmiedestraße 2, 15745 Wildau, Germany

Keywords GNSS · Galileo · Antenna model · Satellite antenna phase center · Orbit modeling

1 Introduction

The space segment of the European global navigation satellite system (GNSS) Galileo currently (mid of December 2015) consists of ten satellites. Four of them belong to the first generation of In-Orbit Validation (IOV) satellites whereas the remaining are so-called Full Operational Capability (FOC) satellites. High-precision geodetic applications require detailed knowledge about the electrical phase center of the satellite antenna. The deviation of this phase center from a well-defined physical reference point is described by phase center offsets (PCOs) and corresponding phase center variations (PCVs) depending on the nadir and azimuth angle of the receiving station as seen from the satellite (e.g., Hofmann-Wellenhof et al. 2008). Usually, the reference point for observation modeling is the center of mass (CoM) of the satellite. The *z*-offset in the antenna's boresight direction (ideally pointing toward the center of the Earth) is also called vertical PCO whereas *x*- and *y*-offsets are called horizontal PCOs. Further details on the spacecraft axis definitions used within the International GNSS Service (IGS; Dow et al. 2009) as well as for this paper are given in Montenbruck et al. (2015a).

Unfortunately, pre-launch ground calibration results for the Galileo satellite antennas are not publicly available neither for the IOV nor the FOC satellites. Therefore, conventional PCO values based on pictures of the satellites and a scale model have been adopted for the Multi-GNSS Experiment (MGEX; Montenbruck et al. 2014) of the IGS for the IOV satellites (Rizos et al. 2013). For the FOC satellites, rounded values of a preliminary PCO estimation based on

Published online: 11 May 2016

Table 1 Galileo satellite antenna PCOs used within MGEX (Montenbruck et al. 2015a) and empirically derived z-offsets for the Galileo broadcast ephemeris (BRDC) as discussed in Sect. 3

Satellite	Type	x (cm)	y (cm)	z (cm)
Galileo IOV	MGEX	−20.0	0.0	+60.0
	BRDC			+75.0
Galileo FOC	MGEX	+15.0	0.0	+100.0
	BRDC			+75.0

a few weeks of data (Steigenberger et al. 2015a) are used so far (Montenbruck et al. 2015a; Schmid 2015). The corresponding numerical values are given in Table 1. Possible PCVs depending on the observation direction are currently neglected for both types of satellites. According to Monjas et al. (2010a), IOV satellites exhibit significant PCVs with peak-to-peak amplitudes of about 10–15 mm for individual frequencies. However, no ground calibrations have been published yet.

The estimation of more accurate PCO values for the Galileo IOV and FOC satellites is a key goal of the present publication. Overall, 20 months of data have been analyzed by two different analysis centers (ACs) and with different orbit modeling strategies. The results are compared and recommendations for updated conventional PCO values for the individual spacecraft types are made. Section 2 introduces the two different generations of Galileo satellites and the two different antenna types used to transmit navigation signals. Section 3 summarizes the estimation of satellite antenna PCOs from global GNSS tracking data and describes the different orbit models applied in the estimation process. The GNSS processing strategies of the two ACs are briefly discussed. The results of the horizontal satellite antenna PCO estimation and the impact of different orbit models on the PCO estimation are shown in Sect. 4 whereas the results for the vertical PCOs are discussed in Sect. 5. Section 6 introduces rounded mean values for the PCOs and evaluates their performance by day boundary discontinuities, orbit fit RMS values, and satellite laser ranging (SLR) residuals. Finally, Sect. 7 summarizes the most important results.

2 The Galileo satellites

Galileo comprises satellites in three orbital planes in medium Earth orbit (MEO) with an inclination of 56° and a semi-major axis of 29,600 km. The eight Galileo satellites considered for this paper are listed in Table 2. The IOV and FOC satellites were built by different manufacturers and are equipped with different types of antenna panels. As for other GNSS satellites, right-hand circularly polarized transmission antennas are used (Chen et al. 2012).

Table 2 Galileo satellites considered for this study

Satellite name	Satellite type	PRN no.	Launch date
GAL-101	IOV-PFM	E11	21 Oct 2011
GAL-102	IOV-FM2	E12	
GAL-103	IOV-FM3	E19	12 Oct 2012
GAL-104[a]	IOV-FM4	E20	
GAL-201[b]	FOC-FM1	E18	22 Aug 2014
GAL-202[b]	FOC-FM2	E14	
GAL-203	FOC-FM3	E26	27 Mar 2015
GAL-204	FOC-FM4	E22	

PRN pseudo-random noise, *PFM* pre-flight model, *FM* flight model
[a] Single-frequency transmission since May 2014
[b] Elliptical orbit due to launch failure

2.1 IOV satellites

The buildup of the operational Galileo constellation started with four IOV satellites manufactured by Airbus Defence & Space (formerly EADS Astrium) that were launched in 2011 and 2012, respectively. In May 2014, GAL-104 experienced a sudden power loss (de Selding 2014) followed by a permanent failure of the E5 and E6 signal transmission. As dual-frequency data are required for the estimation of satellite antenna PCOs, only a limited interval of this satellite can be considered.

The Galileo IOV navigation antenna shown in Fig. 1 is composed of 45 photo-printed stacked patch elements, arranged in six subarrays of six or nine elements with a total diameter of 1.4 m (Arenas et al. 2011; Monjas et al. 2010a, b; Montesano et al. 2007). It is a refinement of the antenna of the second Galileo test satellite, GIOVE-B, which contained 42 patch elements (Rubio et al. 2006).

2.2 FOC satellites

The Galileo FOC satellites are manufactured by OHB System AG (Bremen, Germany). The first pair of satellites (GAL-201 and GAL-202) was launched in August 2014. As a result of

Fig. 1 Galileo IOV transmit antenna. Image courtesy of ESA, Anneke Le Floc'h

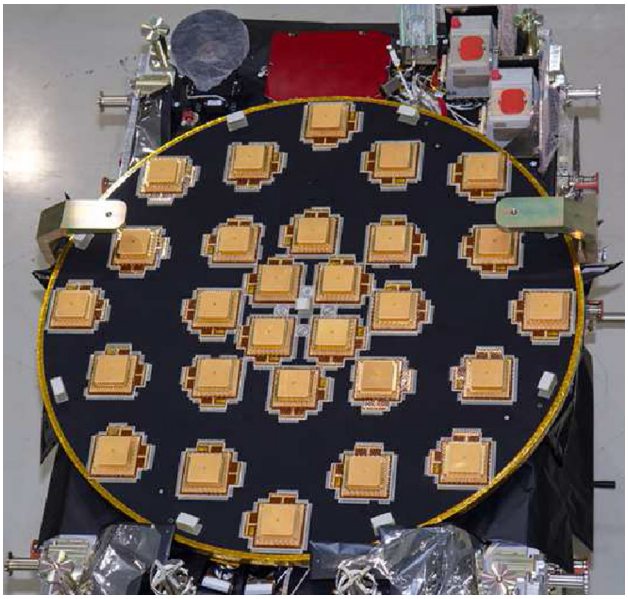

Fig. 2 Galileo FOC transmit antenna. Image courtesy of OHB

a launch anomaly (Arianespace 2014), the spacecraft were injected into an elliptical orbit with an eccentricity of 0.23 and a semi-major axis of 26,200 km instead of a circular orbit with a semi-major axis of 29,600 km. With a series of orbit maneuvers conducted in late 2014 for GAL-201 and early 2015 for GAL-202, the orbits of both satellites could be partly corrected. This resulted in an eccentricity of 0.16, a semi-major axis of 27,980 km, and a 20-day repeat ground track. Signal transmission of both satellites started in December 2014 and March 2015, respectively. The second pair of FOC satellites was launched in March 2015, and signal transmission of GAL-203 and GAL-204 started in late May 2015. However, during summer 2015 extensive transmission outages for up to three FOC satellites occurred. GAL-205 and GAL-206 were not considered for this paper, as they did not start signal transmission before mid of October 2015. Further dual as well as quadruple launches will follow to establish a constellation of 24 operational satellites and up to six active spare satellites (European Union 2014).

The Galileo FOC navigation antenna (Fig. 2) is similar to the antenna of GIOVE-A, the first Galileo test satellite. It comprises an array of 28 stacked patch elements symmetrically arranged in the four quadrants (Valle et al. 2006).

3 Estimation of GNSS satellite antenna parameters

Satellite antenna PCOs and PCVs can be estimated from GNSS observations of a global tracking network together with other parameters like station coordinates, troposphere, orbit, and Earth rotation parameters. However, due to correlations not all parameters can be estimated simultaneously. Strong correlations are, for example, present between:

- terrestrial reference frame scale and z-offsets (Zhu et al. 2003),
- nadir-dependent PCVs and z-offsets (Schmid and Rothacher 2003),
- azimuth-dependent PCVs and horizontal PCOs (Schmid et al. 2005).

Common approaches to cope with these correlations are:

- constraining of the terrestrial scale by a no-net-scale condition w.r.t. the a priori coordinates,
- estimation of PCVs and PCOs in a two-step approach: first, minimized PCVs are determined which are fixed when solving for PCOs.

Furthermore, phase center estimates depend on the geometry of the Sun with respect to the Earth and the satellite, in particular on the elevation angle β of the Sun above the orbital plane. While the nominal attitude control law induces a continuous rotation about the Earth-pointing yaw axis, the variation of the yaw angle decreases with an increasing β-angle. In the theoretical case of $\beta = \pm 90°$, the spacecraft y-axis is aligned with the along-track direction, while the x-axis points toward the Sun. As a consequence, the y-component of the PCO is fully correlated with the orbit parameters. At the same time, the PCO x-component cannot be separated from the direct solar radiation pressure coefficient D_0 (see Sect. 3.2), since both of them induce a shift of the antenna phase center in cross-track direction under the given conditions. The first type of correlation is already well known from the estimation of GPS/GLONASS PCOs and was described, e.g., by Schmid et al. (2007). The second type of correlation, however, becomes more important for Galileo since the stretched shape of the Galileo satellite bodies impacts the solar radiation pressure (SRP) and induces notable variations of D_0 with the β-angle. As a consequence, a proper modeling of the SRP is a prerequisite for a precise determination of Galileo satellite antenna PCOs. Therefore, different SRP models will be applied for the PCO estimation discussed in Sect. 4 to find an optimum estimation strategy.

The satellite antenna corrections of the first absolute IGS antenna phase center model igs05.atx (Schmid et al. 2007) were based on the results of two ACs for GPS and only one for GLONASS. igs05.atx comprised block-specific horizontal and satellite-specific vertical PCOs as well as block-specific nadir-dependent PCVs for the GPS and GLONASS satellites. Due to the difficulties in determining *horizontal* PCOs (see above), manufacturer values were adopted for the IGS antenna model and only z-offsets were estimated.

The current IGS antenna model igs08.atx (Schmid et al. 2015) contains the more recently launched GPS and GLONASS satellites including GPS Block IIF. PCOs and PCVs for the latest generation of GPS satellites were earlier determined by Dilssner (2010). Whereas the horizontal PCOs and the GPS PCVs from igs05.atx and igs08.atx are identical, the vertical PCOs and the GLONASS PCVs (Dach et al. 2011; Dilssner et al. 2010) were updated.

As of July 2015, the values listed in Table 1 for Galileo are also included in igs08.atx (Schmid 2015) together with PCOs for the Chinese BeiDou Navigation Satellite System (BDS), the Japanese Quasi-Zenith Satellite System (QZSS), and the Indian Regional Navigation Satellite System (IRNSS).

For the sake of completeness, we note that PCO values for the Galileo satellites are implicitly contained in the broadcast ephemerides transmitted by those satellites. This is due to the fact that the broadcast orbits transmitted via the navigation message refer to the mean phase center of the satellite rather than the center of mass as for the precise IGS and MGEX ephemeris products. While the PCOs applied by the control center for the generation of broadcast ephemerides are not publicly disclosed, empirical values for the z-offsets could be derived by Montenbruck et al. (2015b) from a comparison of broadcast ephemerides with precise orbit products provided by MGEX. More recent z-offsets valid after the Galileo ground segment update in February and March 2015 (ESA 2015) are listed in Table 1. The analysis is based on five months of data and reveals a change of the IOV z-offset by −10 cm compared to Montenbruck et al. (2015b). The FOC value is based on GAL-203 only, as the other satellites did not start navigation message transmission before November 2015.

3.1 GNSS processing

PCO estimates for the Galileo IOV and FOC satellites obtained by two different institutions are analyzed in this paper:

- German Space Operations Center, Deutsches Zentrum für Luft- und Raumfahrt (DLR),
- IGS Analysis Center of Deutsches GeoForschungsZentrum (GFZ).

A third solution provided by the Center for Orbit Determination in Europe (CODE), hosted by the Astronomical Institute of the University of Bern (AIUB), is exclusively used to provide a fully independent validation in Sect. 6. Details on the DLR orbit determination strategy are given in Montenbruck et al. (2015c) and Steigenberger et al. (2015c). The GFZ solutions build on the contributions of this AC to MGEX (Uhlemann et al. 2015). Table 3 lists general processing options of the two ACs, whereas details on solutions applying different SRP modeling are given in Table 4. The different orbit models are described in Sect. 3.2. Solutions with different orbit modeling cover a limited time interval (DoY 1/2014–181/2015), whereas the final analysis covers an extended interval from DoY 362/2013 to 242/2015.

All ACs employ the ionosphere-free linear combination of L1 and L2 for GPS and of E1 and E5a for Galileo. The observation data comprise combined GPS/Galileo stations from the MGEX network as well as additional legacy IGS stations providing only GPS observations. The GPS satellite antenna PCOs and PCVs were fixed to igs08.atx

Table 3 General analysis options of DLR and GFZ

Solution	DLR	GFZ
Time interval (DoY)	362/2013–242/2015	
Software	NAPEOS 3.3.1[a]	EPOS.P8[b]
Galileo stations	∼70	∼95
GPS stations	∼130	∼110
Sampling rate	5 min	5 min
Elevation cutoff angle	10°	7°
Elevation-dependent weighting[c]	$\sin\epsilon$	$2 \cdot \sin\epsilon$ for $\epsilon < 30°$
Ambiguity fixing	Separately for GPS and Galileo (Ge et al. 2005)	
Datum definition	No-net-rotation with respect to IGb08[d]	
Troposphere a priori model	Global Pressure and Temperature (GPT) model[e]	
Troposphere mapping function	Global Mapping Function (GMF)[f]	

[a] Springer (2009)
[b] Gendt et al. (1999)
[c] ϵ is the elevation
[d] Rebischung et al. (2012) and Rebischung (2012)
[e] Boehm et al. (2007)
[f] Boehm et al. (2006)

Table 4 DLR and GFZ solutions with different SRP modeling

Solution	Orbit parameters	Galileo a priori model	Constraints for D_0	Arc length	
				DLR	GFZ
EC	ECOM, 5 param.	None	None	1 day	3 days
EC2	ECOM-2, 9 param.	None	None	1 day	1 day
BW	ECOM, 5 param.	Box-wing	None	1 day	1 day
BWC	ECOM, 5 param.	Box-wing	0.1 nm/s^2	1 day	n/a

values for all solutions providing a sufficient constraint for the scale. Due to the lack of a complete and consistent set of Galileo receiver antenna calibrations, the GPS L2 PCOs and PCVs were also applied for Galileo E5a. This approximation appears to be justified since anechoic chamber calibrations for selected multi-GNSS antennas reported by Becker et al. (2010) revealed only small PCV differences (e.g., less than 2–5 mm peak-to-peak variation for Trimble Zephyr II and Leica AR25 Rev. 3) for these adjacent frequency bands. Galileo satellite antenna PCOs used within MGEX (Table 1) served as initial values for the data processing. No Galileo satellite antenna PCVs were applied.

Nominal yaw steering (Bar-Sever 1996) is assumed for both IOV and FOC satellites. In reality, the IOV satellites use a so-called dynamic yaw steering (Ebert and Oesterlin 2008) for $|\beta| < 2°$ resulting in deviations of the true attitude from the nominal one for time periods of up to 30 min per revolution during five days in the middle of each eclipse period. However, the impact of these deviations appears to be limited. Our analyses could not show a significant change of the results due to the simplified attitude modeling. For FOC satellites, details of the attitude control have not been disclosed but a similar technique as for IOV can be assumed. For GAL-201/202, larger deviations may, however, apply due to the non-nominal orbit.

3.2 Orbit modeling

Both ACs used established dynamical models in accord with current IGS conventions (IGS ACC 2014). Specific aspects of relevance for the current analysis include the SRP modeling for which different alternatives are considered.

A widely used SRP model is the Empirical CODE Orbit Model (ECOM) developed by Beutler et al. (1994). This model is expressed in a Sun-oriented reference frame with D pointing to the Sun, Y along the solar panel axis and B completing a right-handed system. In each direction, a constant and sine/cosine terms depending on the argument of latitude u are considered resulting in a total number of nine parameters. Usually, only a subset of five parameters is estimated:

$$\begin{aligned} D_{\mathrm{ECOM}} &= D_0 \\ Y_{\mathrm{ECOM}} &= Y_0 \\ B_{\mathrm{ECOM}} &= B_0 + B_C \cdot \cos u + B_S \cdot \sin u \end{aligned} \quad (1)$$

Whereas this model provides a good performance for the GPS satellites, it partly fails for Galileo: analyses of the Galileo products provided by the MGEX ACs revealed systematic errors in the orbit and clock parameters (Steigenberger et al. 2015b) which are related to the different shape of the Galileo satellites compared to GPS. Two different approaches have been developed to cope with these systematic errors. The first introduces an a priori model accounting for the specific properties of the Galileo satellites whereas the second considers additional parameters to be estimated.

Montenbruck et al. (2015c) developed an a priori box model for the Galileo IOV satellites accounting for the optical properties and dimensions of the satellites. Accelerations in D- and B-direction are modeled as a function of the Sun elongation (angle between Earth and Sun as seen from the satellite). In the following, this model is used for both the IOV and FOC satellites with an additional a priori acceleration of $D_0 = 87$ nm/s^2 applied. This model is labeled as box-wing (BW) model. The BW model is employed as an a priori model along with the five-parameter ECOM to compensate any remaining deficiency of a BW-only SRP model.

Arnold et al. (2015) modified and extended the ECOM by changing the angular argument to the orbit angle with respect to orbit noon Δu and by adding higher order even harmonics in D-direction and odd harmonics in B-direction. The orbit model labeled as ECOM-2 in this paper considers only the 2nd and 4th order harmonics in D-direction:

$$\begin{aligned} D_{\text{ECOM-2}} = D_0 &+ D_{C2} \cdot \cos 2\Delta u + D_{S2} \cdot \sin 2\Delta u \\ &+ D_{C4} \cdot \cos 4\Delta u + D_{S4} \cdot \sin 4\Delta u \end{aligned} \quad (2)$$

Both approaches provide a significant reduction of the systematic orbit and clock errors and have a similar performance. It must be noted, however, that the ECOM-2 parameters exhibit notable seasonal (β-dependent) variations and do not enable a simple constraining of the estimated parameters. The BW a priori model, in contrast, accounts for most of the β-angle variation and can thus be used with constrained empirical parameters.

4 Estimation of *x*- and *y*-offsets

Although horizontal and vertical PCOs were estimated simultaneously, they are discussed in different sections (Sects. 4, 5) due to their different characteristics. Furthermore, the horizontal PCOs of Galileo IOV and FOC satellites also show a different behavior (Sects. 4.1, 4.2).

4.1 Galileo IOV satellites

4.1.1 PCO time series

GAL-103 was selected as an example for the Galileo IOV satellites as it covers the widest range of β-angles ($-74.7°$ to $+75.6°$, see Fig. 3a). The three other IOV satellites exhibit a similar behavior. However, β-dependent systematic effects are less pronounced for GAL-101 and GAL-102 as these satellites are in a different orbital plane and experience a smaller range of β-angles ($-61.8°$ to $+63.5°$).

Figure 3b shows the *x*-offset estimates of DLR and GFZ based on the ECOM five-parameter model without any a priori model (solution EC). Both solutions reveal a pronounced periodic signal with a peak-to-peak amplitude of almost 70 cm. Estimates close to the conventional MGEX value of -20 cm, which approximates the geometric antenna center with an uncertainty of 5–10 cm, only occur for very short time periods when the β-angle is close to zero.

The largest deviations of the *x*-offset estimates from the conventional value are detected during time periods with large absolute values of the β-angle (e.g., in January 2015). The DLR solution shows a slightly larger scatter compared to GFZ which can be attributed to different arc lengths (1 day vs. 3 days, see Table 4). The clear dependence of the *x*-offset estimates on the β-angle indicates deficiencies/correlations with the SRP parameters which will be discussed later.

The *x*-offset estimates based on the more sophisticated ECOM-2 model (solution EC2) displayed in Fig. 3c show a quite different behavior compared to solution EC. Both the DLR and the GFZ solution provide stable *x*-offset estimates with a scatter of less than 10 cm during short periods with $|\beta| < 20°$. Outside this range, the scatter of both solutions increases dramatically with peak-to-peak variations of up to 2.5 m. Obviously, the extended parameterization of ECOM-2 with 9 SRP parameters is not appropriate for the simultaneous estimation of PCOs and orbit parameters.

The positive impact of the a priori box-wing model is demonstrated in Fig. 3d which exhibits a completely different pattern compared to all other solutions discussed so far. The periods with stable PCO estimates are much longer. Only during periods of about one month around the extreme β-angles, a larger scatter as well as deviations of up to 40 cm from the conventional MGEX value occur. The GFZ BW solution (not shown in Fig. 3d) has a similar performance.

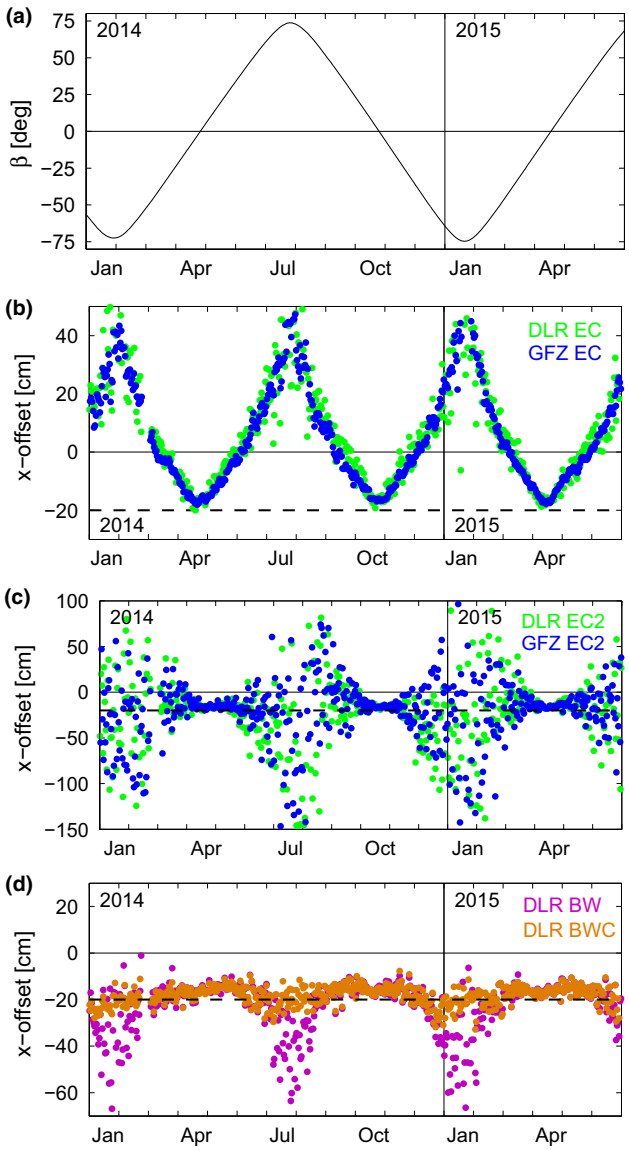

Fig. 3 Time series for GAL-103: **a** elevation β of the Sun above the orbital plane; **b** DLR and GFZ *x*-offset estimates based on the ECOM five-parameter model; **c** DLR and GFZ *x*-offset estimates based on the ECOM-2 model; **d** DLR *x*-offset estimates based on the ECOM five-parameter model and the a priori box-wing model without (BW) and with constraints (BWC) for D_0. In each case, the *dashed line* indicates the conventional MGEX value of -20 cm

Analyses of the correlation matrix obtained from the least squares adjustment confirm strong correlations of the *x*-offsets with the direct SRP parameter D_0. Figure 4a shows the D_0 parameter for a DLR solution applying the a priori box-wing model *without* estimating PCOs. The largest absolute D_0 values occur for $|\beta| > 60°$ which coincides with increased formal errors of the PCO estimates in solution BW (see Fig. 5). The estimated D_0 values exhibit a standard deviation (STD) of 0.5 nm/s^2. This comparatively low STD is related to the proper SRP modeling achieved by the box-wing

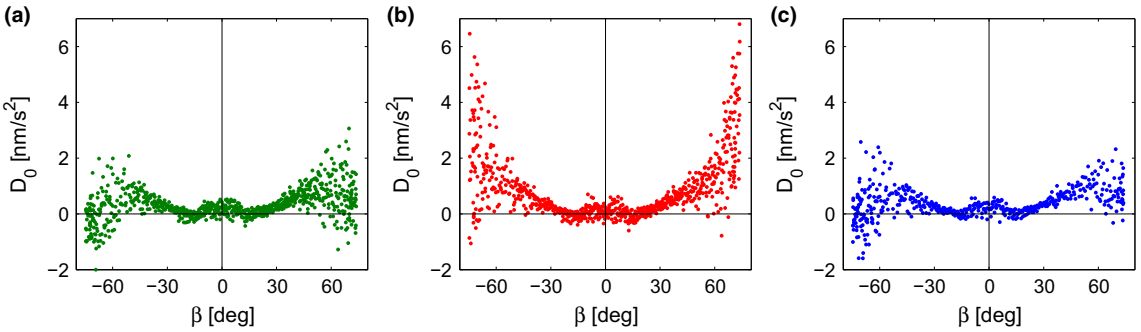

Fig. 4 Direct solar radiation pressure parameter D_0 vs. elevation β of the Sun above the orbital plane for GAL-103: **a** DLR solution based on box-wing model but without estimation of PCOs; **b** DLR solution with estimation of PCOs (DLR BW); **c** DLR solution with estimation of PCOs and a constraint of 0.1 nm/s^2 for D_0 (DLR BWC)

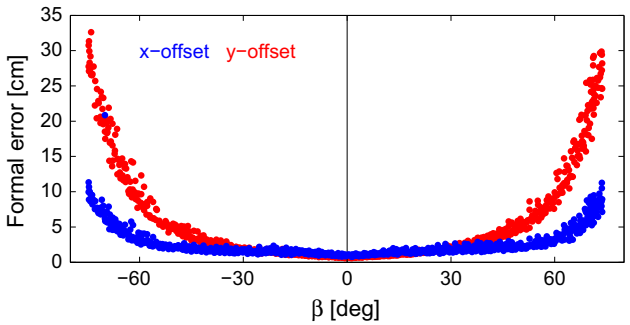

Fig. 5 Formal errors of the horizontal satellite antenna PCO estimates vs. elevation β of the Sun above the orbital plane for GAL-103 in solution DLR BW

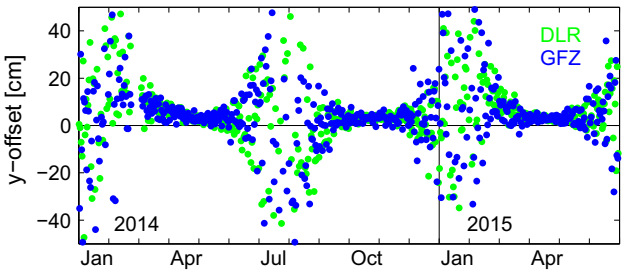

Fig. 6 GAL-103 satellite antenna y-offsets resulting from solution BW

model. In contrast, a solution with five-parameter ECOM but without the a priori box-wing model exhibits an STD for D_0 of 2.4 nm/s^2 with a peak-to-peak variation of 8 nm/s^2.

As soon as horizontal PCOs are estimated (Fig. 4b), the D_0 scatter increases resulting in an STD of 1.1 nm/s^2. Different constraints for D_0 were analyzed when estimating PCOs to stabilize the D_0 estimates and to improve the x-offset results. A constraint of 0.1 nm/s^2 is considered most appropriate as it results in a D_0 behavior (Fig. 4c) that is very similar to the solution without PCO estimation. The impact of the D_0 constraint on the x-offset estimates is shown in Fig. 3d. Outliers during periods with large absolute values of the β-angle can be significantly reduced. Note that the constraining of D_0 is only possible with the a priori box-wing model but neither with stand-alone ECOM nor ECOM-2, since both models yield β-dependent D_0 estimates due to the stretched bodies of the Galileo satellites.

Figure 6 shows the y-offset estimates for GAL-103 resulting from solution BW. Only time periods with low β-angles provide stable y-offset estimates whereas variations of up to $\pm$50 cm appear for periods with large absolute values of the β-angle. In contrast to the x-offsets, solutions with different SRP modeling (Table 4) do not differ significantly.

The β-dependence of the formal errors of the horizontal Galileo PCO estimates in Fig. 5 is similar to the GPS results of Schmid et al. (2007) but the maximum Galileo values are larger by a factor of about two. As already mentioned in Sect. 3, the formal errors mainly reflect the determinability of the PCOs due to the satellite/Sun geometry which is similar for GPS and Galileo. The formal errors of the GFZ solution BW are slightly smaller but show the same shape. The worse performance of the Galileo PCO estimation compared to GPS might be related to the inferior ambiguity resolution rate due to the incomplete satellite constellation. Whereas 98 % of the GPS ambiguities could be fixed in the DLR solution, the Galileo ambiguity resolution rate varies between 30 and 85 % with an average of 70 %.

4.1.2 Mean PCO values

Whereas the analysis of time series is important to identify systematic effects, the final result of a PCO estimation should be a single set of PCO values per satellite or satellite group. Based on the results presented so far, several methods could be applied to derive the desired PCO values:

- weighted average (either simple averaging based on formal errors or combination of normal equations),

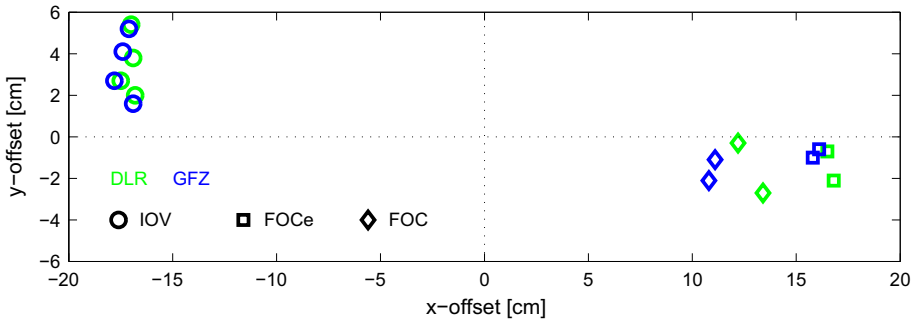

Fig. 7 Mean horizontal Galileo satellite antenna offsets. FOCe stands for the Galileo FOC satellites with *elliptical* orbit, namely GAL-201 and -202

- unweighted average but exclusion of time periods with systematic effects (selection based on β-angle or formal errors),
- unweighted average of solution BWC with D_0 constraint.

All three methods agree within a few millimeters. Therefore, the unweighted average of solution BW with exclusion of time periods with $|\beta| > 50°$ was selected as it can be easily applied without determining AC-specific outlier limits and as no GFZ solution with D_0 constraint was available. The mean horizontal PCOs per satellite and AC for the extended analysis interval (see Sect. 3.1) are plotted in Fig. 7. The mean horizontal IOV PCOs of DLR and GFZ agree within 5 mm. The differences between individual satellites are larger than the AC-specific differences and reach 1 cm in the x-component and 3.5 cm in the y-component, respectively.

4.2 Galileo FOC satellites

4.2.1 PCO time series

For Galileo FOC satellites, only limited tracking data were available, as the first satellite did not start signal transmission before December 2014. Furthermore, all satellites were affected by transmission outages of up to several weeks. Here, the extended time interval of solution BW is considered. As GAL-201 is the satellite with the longest observation history, this satellite is used for illustration purposes. The short data set of about 8 months in Fig. 8 shows that the systematic effects visible in the IOV x-offset estimates (Fig. 3d) do not appear in the FOC time series. In contrast to IOV, the FOC x-offset is positive. The y-offset estimates (Fig. 8c) reveal a dependence of the scatter on β (maximum β-angle of 48.9° in late March 2015, β equal zero in early January and late June 2015). The formal errors of the horizontal PCOs of the Galileo FOC satellites (not shown here) are very similar to the IOV estimates (Fig. 5), although the maximum β-angle of GAL-201 is comparatively small.

Small systematic effects are visible in the horizontal PCOs of GAL-201/202 for $|\beta| < 5°$ (end of June 2015; another period with β close to 0° at the end of 2014 coincides with a transmission outage). For the x-offsets, a systematic bias of about 5 cm appears, whereas the y-offset shows a sinusoidal behavior with a peak-to-peak amplitude of about 8 cm during a time period of about 16 days. These effects are probably related to a modified behavior of the attitude control system due to the high eccentricity of the orbits of these satellites. GAL-203 and GAL-204 flying in a nominal orbit with almost zero eccentricity do not show such a behavior.

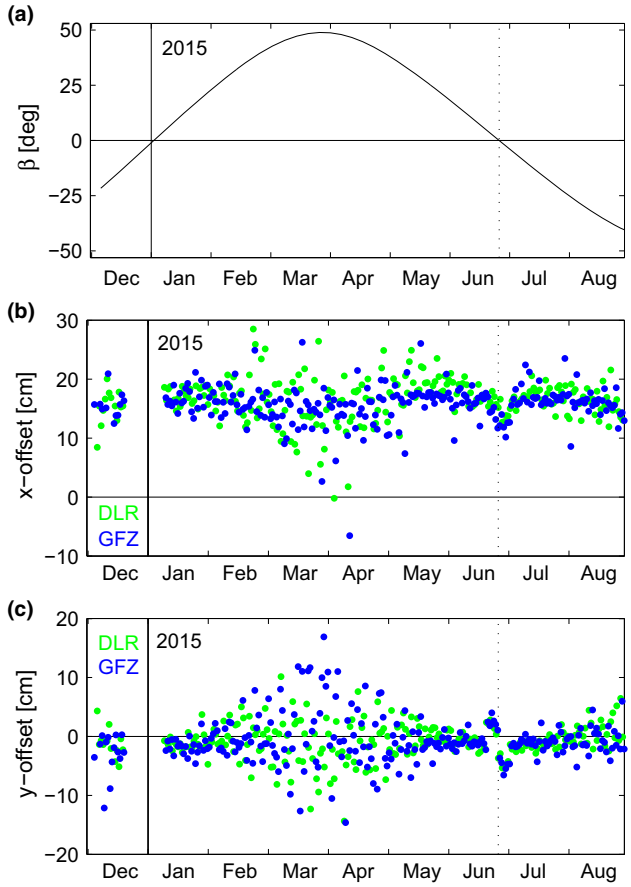

Fig. 8 Time series for GAL-201 resulting from solution BW: **a** elevation β of the Sun above the orbital plane; **b** x-offsets; **c** y-offsets. The *dotted vertical line* marks $\beta = 0°$

4.2.2 Mean PCO values

The mean offsets of GAL-201 and GAL-202 (labeled as FOCe in Fig. 7) agree to about 1 cm. The scatter of GAL-203 and GAL-204 (labeled as FOC) is larger with maximum PCO differences of up to 2.5 cm. However, one has to keep in mind that these PCO estimates are based on only a few weeks of data (7 weeks for GAL-203 and 2.5 weeks for GAL-204). A mean difference of about 4 cm can be detected between the x-offsets of GAL-201/202 and GAL-203/204 which is related to the significantly different masses of these satellites.

The CoM values published on the web page of the International Laser Ranging Service (ILRS 2015) allow for an assessment of the PCO change due to fuel consumption. GAL-201 and GAL-202 used a notable portion of their fuel to reduce the eccentricity of their orbits. The mass loss due to these maneuvers was about 45 kg. This can be inferred from the comparison of the begin of life masses of the four FOC satellites as published by the ILRS (2015). The large mass difference allows for an evaluation of the impact of mass loss on the PCO. Differentiating the CoM values and the masses of GAL-201/202 and GAL-203/204 results in x-offset changes of 1.2–1.6 mm/kg. The impact on the y- and z-offsets is negligible: less than 0.1 mm/kg and 0.03 mm/kg, respectively.

Based on a mean change of 1.4 mm/kg, the x-offsets of GAL-201/202 should differ by 6.3 cm from GAL-203/204 which is 50 % larger than the estimated difference of 4 cm. This discrepancy might be due to uncertainties in the PCO estimation or in the calculation of the CoM values. However, the consideration of different x-offset values for GAL-201/202 and GAL-203/204 is appropriate as the estimated difference is larger than the estimation uncertainty.

The mass difference between satellites within the same orbital plane is 1.7 kg for GAL-201/202 and 0.5 kg for GAL-203/204, respectively. For future quadruple launches with Ariane V, which should start in 2016, larger mass differences between the four satellites distributed within one orbital plane may be expected. However, even for differences of 3 kg the impact on the x-offset would be less than 5 mm which still appears negligible from a practical point of view.

5 Estimation of z-offsets

5.1 PCO time series

Figure 9 shows the vertical PCO estimates for GAL-103 resulting from solution BW of DLR and GFZ. In general, the z-offset estimates have a larger scatter than the horizontal PCOs but they do not exhibit pronounced systematic effects. The STDs of the time series are on the 15–20 cm level for both types of satellites and different ACs. Exceptions are the

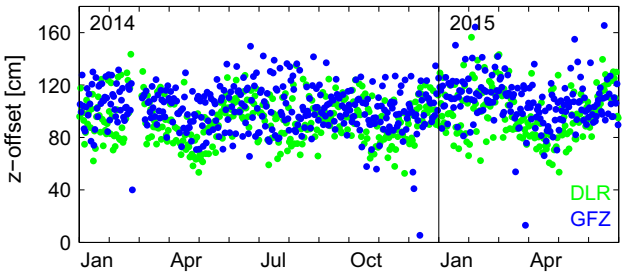

Fig. 9 GAL-103 satellite antenna z-offset estimates resulting from solution BW

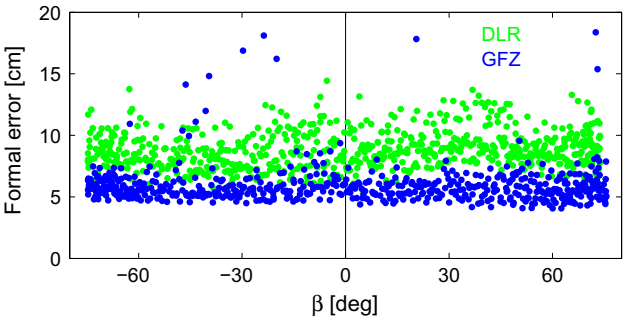

Fig. 10 Formal errors of the GAL-103 satellite antenna z-offset estimates vs. elevation β of the Sun above the orbital plane resulting from solution BW

STD of 28 cm for GAL-204 estimates of DLR (based on only 2.5 weeks of data) and of 25 cm for the GAL-103 estimates of GFZ. The z-offset bias between the two ACs of about 10 cm that is better visible in Fig. 11 will be discussed in Sect. 5.2.

The formal errors of the z-offsets of GAL-103 are plotted in Fig. 10 for solution BW of both DLR and GFZ. The mean formal errors are on the level of about 8 cm for DLR and 6 cm for GFZ. A comparison of these formal errors with the actual scatter of the corresponding time series reveals that the formal errors are too optimistic by a factor of 2–3. Compared to the formal errors of the x- and y-offsets (Fig. 5), those of the z-offsets are also more scattered but do neither show a systematic pattern nor a dependence on β. No general differences can be detected between the z-offset time series of the FOC satellites and those of the IOV satellites, neither for the PCO estimates nor the formal errors. In contrast to the horizontal PCOs, different orbit modeling has a negligible impact on the z-offset estimation.

5.2 Mean PCO values

The formal errors of the z-offset estimates were introduced as weights for the computation of mean values from the individual time series of the two ACs. These mean values are plotted in Fig. 11. The mean differences between DLR and GFZ are on the level of -9 to -15 cm for the IOV and $+2$ to $+6$ cm for the FOC satellites. The different sign of the AC-specific

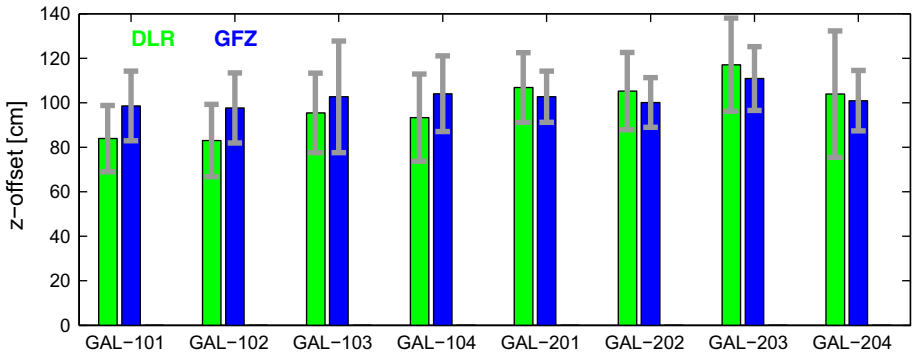

Fig. 11 Mean Galileo satellite antenna z-offsets based on solution BW. The *gray bars* indicate the STD of the corresponding time series

Table 5 Rounded average Galileo satellite antenna PCOs based on the DLR and GFZ analyses

Satellite	x (cm)	y (cm)	z (cm)
Galileo IOV	−17	+3	+95
GAL-201/202	+16	−1	+105
GAL-203/204	+12	−1	+110

bias for IOV and FOC renders a general scale difference between the DLR and GFZ solutions unlikely. Schmid et al. (2015) report mean differences in the GPS z-offset estimates of five different ACs of 6.4 cm and a maximum of 22 cm. Like for the horizontal PCOs, the worse agreement of the vertical Galileo PCO estimates between different ACs compared to GPS might be attributed to the ambiguity resolution rate (see Sect. 4.1.1). The AC-specific mean z-offsets of the IOV satellites within the same orbital plane (GAL-101/102 and GAL-103/104) differ by only 1 cm except for the DLR values of GAL-103/104 that differ by 3 cm.

6 Galileo PCO model and model validation

Due to the uncertainties of the PCO estimates discussed in the previous sections, specifying individual and precise values for each satellite seems not justified at present. Therefore, rounded values for three different groups of Galileo satellites are proposed in Table 5. Whereas the individual IOV satellites do not show significant differences, two subgroups have to be formed for the FOC satellites due to significantly different x-components of the PCOs (see Sect. 4.2.2): the satellites in nominal (GAL-203/204) and the satellites in elliptical orbit (GAL-201/202). The PCO values to be rounded were weighted mean values of both DLR and GFZ. To account for the different lengths of the time series, the number of PCO estimates was used as weight. The formal errors of the mean values are on the 1–2 cm level for the horizontal PCOs and the 1 dm level for the z-offsets. Therefore, the horizontal PCOs were rounded to 1 cm whereas the vertical PCOs were rounded to 5 cm.

For the validation of this model, half a year (DoY 60–242/2015) of Galileo orbits were reprocessed with the MGEX model (Table 1) and the newly estimated PCO model (Table 5). The NAPEOS software was used with the same options as described in Sect. 3.1 (solution DLR BW) except for the estimation of PCO parameters. In addition, for a fully independent assessment, identical computations were performed with the Bernese GNSS Software (Dach et al. 2015) by AIUB.

Three different quantities are listed in Table 6 for the evaluation of the orbit quality (detailed description can be found in Steigenberger et al. 2015b):

- Day boundary discontinuities (DBDs): 3D position differences between two consecutive orbits at the midnight epoch.
- Orbit fit RMS: RMS of differences between orbit positions from two (NAPEOS) or three (Bernese) consecutive 1-day orbits with respect to a 2-day/3-day fit through these orbits.
- SLR residuals: offset and standard deviation of one-way SLR range residuals. The orbits estimated from GNSS microwave observations and SLRF2008 (Pavlis 2009) station coordinates are kept fixed and residuals are computed with DLR's GPS High-Precision Orbit Determination Software Tools (GHOST; Wermuth et al. 2010).

A clear improvement by about one third can be seen for the DBDs of the IOV orbits computed with the new model and the NAPEOS software. For the FOC satellites, the improvement is only on the 1–2 cm level due to the much smaller z-offset differences between the two phase center models ($\Delta z = 5$ and 10 cm for FOC compared to 35 cm for IOV). The orbit fit RMS values resulting from the validation with NAPEOS can also benefit from the new PCO model, but only on the few millimeter level. Again, the IOV satellites show a larger improvement than the FOC satellites. When switching to the new PCO model, the absolute value of the SLR offset increases by 1.5 cm for the IOV satellites but only by a few millimeters for the FOC satellites. In general, the STD

Table 6 Validation of the new Galileo satellite antenna PCO model for a half-year period (DoY 60–242/2015)

Solution	Satellite	Day boundary Discont. (cm)		Orbit fit RMS (cm)		SLR residuals Offset (cm)		STD (cm)	
		MGEX	New	MGEX	New	MGEX	New	MGEX	New
NAPEOS	GAL-101	24.2	16.1	6.0	5.5	−1.7	−3.3	3.5	3.3
	GAL-102	24.0	16.0	6.0	5.7	−2.1	−3.6	3.6	3.3
	GAL-103	28.1	18.6	6.0	5.6	−1.3	−2.8	3.6	3.5
	GAL-201	13.5	12.2	4.8	4.7	−2.2	−2.5	2.8	2.8
	GAL-202	14.9	14.4	5.0	5.0	−2.6	−2.9	3.1	3.2
	GAL-203	21.8	19.6	6.5	6.4	−2.1	−2.0	3.7	3.2
	GAL-204	20.3	19.6	7.0	6.7	−3.0	−2.8	5.5	5.9
Bernese	GAL-101	20.8	14.0	5.0	4.5	−2.2	−3.9	4.3	3.9
	GAL-102	18.5	13.8	4.8	4.5	−2.6	−4.0	5.0	4.4
	GAL-103	20.8	15.8	5.6	5.0	−1.6	−3.5	4.6	4.4
	GAL-201	14.1	15.3	4.1	4.3	−3.4	−3.8	5.0	4.7
	GAL-202	14.8	16.2	4.5	4.6	−3.1	−3.5	5.1	5.0
	GAL-203	22.1	20.0	6.3	6.2	−2.8	−2.4	7.2	6.0
	GAL-204	39.4	33.6	13.3	13.7	−0.7	0.2	8.4	8.7

Columns *MGEX* refer to the PCO values in Table 1, columns *New* to Table 5

decreases by up to 5 mm. The only exceptions are GAL-202 and GAL-204 with a degradation of 1 and 4 mm, respectively. However, the results for GAL-204 are based on the smallest data set of only 200 normal points which is reflected in an STD of about 6 cm. It may be noted that the occurrence of increased SLR offsets is evidently counterintuitive and contradicts the presumed improvement of the orbits when using the new PCO model. However, it needs to be emphasized that the estimated SLR offsets may be affected by a variety of other effects such as erroneous laser retroreflector offsets with respect to CoM or SRP modeling errors. The small offset obtained with the MGEX PCO values might, therefore, reflect a cancelation of two opposite error sources. It is, therefore, difficult at present to employ the mean SLR offset as a criterion for the benefit of refined PCOs.

The Bernese validation provides a slightly different picture. Whereas the DBD improvements due to the new model are on the NAPEOS level for the IOV satellites and the FOC satellites in nominal orbit, a degradation of about 1.5 cm occurs for the FOC satellites in elliptical orbit. Slightly increased orbit fit RMS values can be detected for the same satellites whereas the other RMS values decrease on the few millimeter level except for GAL-204. The SLR offsets resulting from the Bernese validation generally differ by about −0.5 cm compared to the NAPEOS validation. However, the degradation in the SLR offsets when switching to the new PCO model as well as the STD improvements are very similar for both validations.

Overall, the validation using two independent software packages confirms a modest benefit from the new PCO values for the precision of Galileo orbit products. However, it is also evident that those products have not yet reached the same level of accuracy as presently achieved for GPS. Despite all the effort to employ common processing standards, solutions obtained with different software packages still reveal subtle differences which potentially mask the benefit from the revised PCO estimates. Thus, a further refinement of the Galileo orbit modeling (e.g., attitude models, radiation pressure) is deemed necessary. PCO estimates presented in this work are, therefore, subject to further revision as improved models and longer data arcs become available. This is particularly true for the FOC satellites which have only be observed for a fairly limited time span so far.

7 Summary and outlook

Satellite antenna PCOs for the Galileo IOV and FOC satellites were estimated by two different ACs. The agreement of the mean horizontal PCOs between solutions of both ACs is on the few millimeter level for the IOV and on the 1–2 cm level for the FOC satellites. Due to a significantly different mass, two groups of FOC satellites have to be distinguished as regards the x-offset: the pair of FOC satellites in elliptical and the FOC satellites in nominal orbit with an x-offset differing by about 4 cm.

The stretched body of the Galileo satellites requires an appropriate orbit modeling for a proper determination of the horizontal PCOs. The estimation of 5 ECOM parameters and the consideration of an a priori box-wing model gave the most stable PCO estimates. Nevertheless, pronounced systematic effects depending on the elevation of the Sun above the orbital plane are still present in this solution. Therefore, time inter-

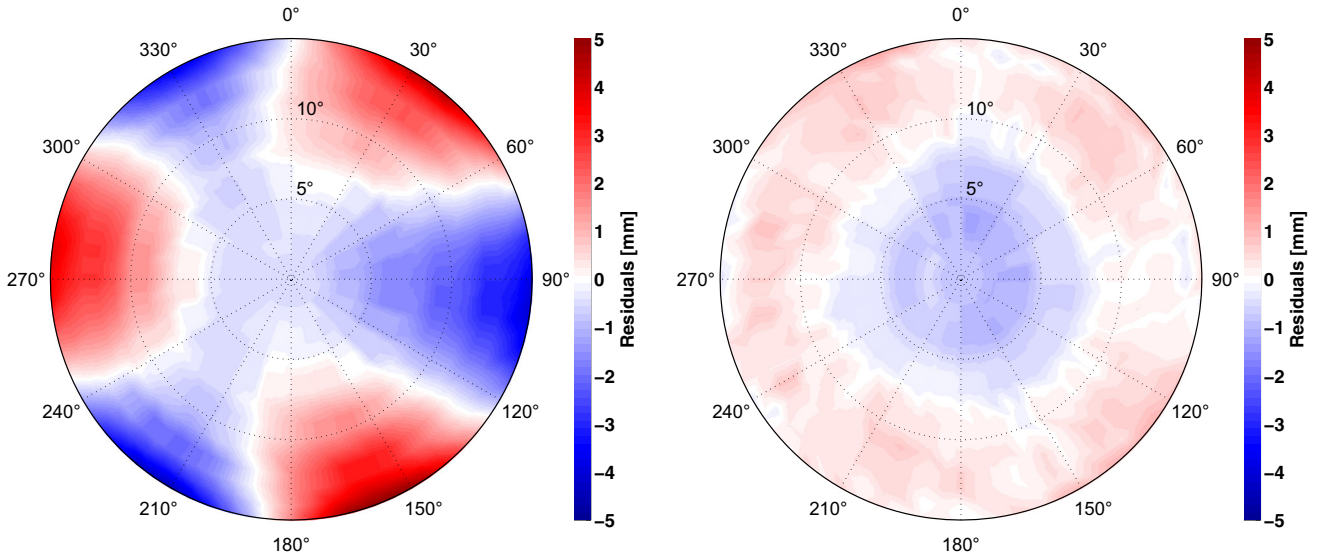

Fig. 12 Mean phase residual maps of Galileo IOV (*left*) and FOC (*right*) obtained from the extended analysis interval

vals with large absolute values of the β-angle were excluded for the determination of mean values per satellite group.

Distinct differences between the IOV and FOC satellites are also visible in the phase residual maps (Fig. 12). For IOV, a clear threefold pattern with an amplitude of 5 mm is visible. The shape of the pattern is probably related to the design of the IOV antennas which are composed of three 6-element and three 9-element subarrays. The single-frequency radiation patterns reported by Monjas et al. (2010a) are very similar although their amplitude is bigger by a factor of two. The FOC residuals do not show an azimuth-dependence but only a small nadir-dependent pattern with maximum values of ± 1 mm. The pronounced threefold pattern in the IOV residual maps suggests the presence of significant PCVs. Therefore, the estimation of PCVs for this satellite type will be one of the next steps in refining the Galileo satellite antenna model.

Acknowledgments The IGS MGEX is acknowledged for providing GNSS observation data. We also thank the European Space Agency for granting access to the NAPEOS software version 3.3.1.

References

Arenas S, Monjas F, Montesano A, Montesano C, Mangenot C, Salghetti L (2011) Performances of GALILEO system navigation antenna for global positioning. In: Proceedings of the Fifth European Conference on Antennas and Propagation (EuCAP 2011), IEEE, pp 1018–1022

Arianespace (2014) Galileo satellites experience orbital injection anomaly on Soyuz launch: initial report. Press release. http://www.arianespace.com/press-release/galileo-satellites-experience-orbital-injection-anomaly-on-soyuz-launch-initial-report. Accessed 10 May 2016

Arnold D, Meindl M, Beutler G, Dach R, Schaer S, Lutz S, Prange L, Sośnica K, Mervart L, Jäggi A (2015) CODE's new solar radiation pressure model for GNSS orbit determination. J Geod 89(8):775–791. doi:10.1007/s00190-015-0814-4

Bar-Sever YE (1996) A new model for GPS yaw attitude. J Geod 70(11):714–723. doi:10.1007/BF00867149

Becker M, Zeimetz P, Schönemann E (2010) Anechoic chamber calibrations of phase center variations for new and existing GNSS signals and potential impacts in IGS processing. In: IGS Workshop 2010, Newcastle

Beutler G, Brockmann E, Gurtner W, Hugentobler U, Mervart L, Rothacher M, Verdun A (1994) Extended orbit modeling techniques at the CODE processing center of the international GPS service for geodynamics (IGS): theory and initial results. Manuscr Geod 19:367–386

Boehm J, Niell A, Tregoning P, Schuh H (2006) Global Mapping Function (GMF): a new empirical mapping function based on numerical weather model data. Geophys Res Lett 33(7):L07304. doi:10.1029/2005GL025546

Boehm J, Heinkelmann R, Schuh H (2007) Short note: a global model of pressure and temperature for geodetic applications. J Geod 81(10):679–683. doi:10.1007/s00190-007-0135-3

Chen X, Parini CG, Collins B, Yao Y, Rehman MU (2012) Antennas for global navigation satellite systems. Wiley, New York

Dach R, Schmid R, Schmitz M, Thaller D, Schaer S, Lutz S, Steigenberger P, Wübbena G, Beutler G (2011) Improved antenna phase center models for GLONASS. GPS Solut 15(1):49–65. doi:10.1007/s10291-010-0169-5

Dach R, Lutz S, Walser P, Fridez P (eds) (2015) Bernese GNSS Software Version 5.2. Astronomical Institute, University of Bern, Switzerland. doi:10.7892/boris.72297

de Selding PB (2014) ESA proceeding with Galileo launches despite in-orbit satellite issues. SpaceNews. http://spacenews.com/41616esa-proceeding-with-galileo-launches-despite-in-orbit-satellite-issues. Accessed 10 May 2016

Dilssner F (2010) GPS IIF-1 satellite: antenna phase center and attitude modeling. Inside GNSS 5(6):59–64

Dilssner F, Springer T, Flohrer C, Dow J (2010) Estimation of phase center corrections for GLONASS-M satellite antennas. J Geod 84(8):467–480. doi:10.1007/s00190-010-0381-7

Dow JM, Neilan RE, Rizos C (2009) The International GNSS Service in a changing landscape of Global Navigation Satellite Systems. J Geod 83(3–4):191–198. doi:10.1007/s00190-008-0300-3

Ebert K, Oesterlin W (2008) Dynamic yaw steering method for spacecraft. European patent specification EP 1526072B1

ESA (2015) Galileo system updated and back to work. http://www.esa.int/Our_Activities/Navigation/Galileo_system_updated_and_back_to_work. Accessed 10 May 2016

European Union (2014) European GNSS (Galileo) open service: signal in space interface control document. OS SIS ICD Issue 1.2

Ge M, Gendt G, Dick G, Zhang FP (2005) Improving carrier-phase ambiguity resolution in global GPS network solutions. J Geod 79(1–3):103–110. doi:10.1007/s00190-005-0447-0

Gendt G, Dick G, Söhne W (1999) GFZ analysis center of IGS – annual report 1998. In: Gowey K, Neilan R, Moore A (eds) IGS 1998 Technical Reports, Jet Propulsion Laboratory, pp 79–87

Hofmann-Wellenhof B, Lichtenegger H, Wasle E (2008) GNSS – global navigation satellite systems: GPS, GLONASS, Galileo & more, 1st edn. Springer, Wien

IGS ACC (2014) International GNSS Service 2nd data reprocessing campaign. http://acc.igs.org/reprocess2.html. Accessed 10 May 2016

ILRS (2015) Galileo center of mass information. http://ilrs.gsfc.nasa.gov/missions/satellite_missions/current_missions/ga01_com.html. Accessed 10 May 2016

Monjas F, Montesano A, Arenas S (2010a) Group delay performances of Galileo system navigation antenna for global positioning. In: 32nd ESA Antenna Workshop on Antennas for Space Applications, Noordwijk

Monjas F, Montesano A, Montesano C, Llorente JJ, Cuesta LE, Naranjo M, Arenas S, Madrazo I, Martínez L (2010b) Test campaign of the IOV (In Orbit Validation) Galileo system navigation antenna for global positioning. In: Proceedings Fourth European Conference on Antennas and Propagation (EuCAP 2010). IEEE, New York

Montenbruck O, Steigenberger P, Khachikyan R, Weber G, Langley RB, Mervart L, Hugentobler U (2014) IGS-MGEX: preparing the ground for multi-constellation GNSS science. Inside GNSS 9(1):42–49

Montenbruck O, Schmid R, Mercier F, Steigenberger P, Noll C, Fatkulin R, Kogure S, Ganeshan AS (2015a) GNSS satellite geometry and attitude models. Adv Space Res 56(6):1015–1029. doi:10.1016/j.asr.2015.06.019

Montenbruck O, Steigenberger P, Hauschild A (2015b) Broadcast versus precise ephemerides: a multi-GNSS perspective. GPS Solut 19(2):321–333. doi:10.1007/s10291-014-0390-8

Montenbruck O, Steigenberger P, Hugentobler U (2015c) Enhanced solar radiation pressure modeling for Galileo satellites. J Geod 89(3):283–297. doi:10.1007/s00190-014-0774-0

Montesano A, Montesano C, Caballero R, Naranjo M, Monjas F, Cuesta LE, Zorrilla P, Martínez L (2007) Galileo system navigation antenna for global positioning. In: Proceedings of the Second European Conference on Antennas and Propagation (EuCAP 2007)

Pavlis E (2009) SLRF2008: the ILRS reference frame for SLR POD contributed to ITRF2008. In: 2009 Ocean Surface Topography Science Team Meeting, Seattle

Rebischung P (2012) IGb08: an update on IGS08. IGSMAIL-6663. https://igscb.jpl.nasa.gov/pipermail/igsmail/2012/007853.html. Accessed 10 May 2016

Rebischung P, Griffiths J, Ray J, Schmid R, Collilieux X, Garayt B (2012) IGS08: the IGS realization of ITRF2008. GPS Solut 16(4):483–494. doi:10.1007/s10291-011-0248-2

Rizos C, Montenbruck O, Weber R, Weber G, Neilan R, Hugentobler U (2013) The IGS MGEX experiment as a milestone for a comprehensive multi-GNSS service. In: Proceedings of the ION 2013 Pacific PNT meeting, pp 289–295

Rubio J, González MA, Zapata J, Montesano A, Monjas F, Cuesta LE (2006) Full-wave analysis of the Galileo system navigation antenna by means of the generalized scattering matrix of a finite array. In: Proceedings of the First European Conference on Antennas and Propagation (EuCAP 2006). doi:10.1109/EUCAP.2006.4584554

Schmid R (2015) igs08_1854.atx: Update including Galileo, BeiDou, QZSS and IRNSS satellites. IGSMAIL-7126. https://igscb.jpl.nasa.gov/pipermail/igsmail/2015/008316.html. Accessed 10 May 2016

Schmid R, Rothacher M (2003) Estimation of elevation-dependent satellite antenna phase center variations of GPS satellites. J Geod 77(7–8):440–446. doi:10.1007/s00190-003-0339-0

Schmid R, Rothacher M, Thaller D, Steigenberger P (2005) Absolute phase center corrections of satellite and receiver antennas: impact on global GPS solutions and estimation of azimuthal phase center variations of the satellite antenna. GPS Solut 9(4):283–293. doi:10.1007/s10291-005-0134-x

Schmid R, Steigenberger P, Gendt G, Ge M, Rothacher M (2007) Generation of a consistent absolute phase center correction model for GPS receiver and satellite antennas. J Geod 81(12):781–798. doi:10.1007/s00190-007-0148-y

Schmid R, Dach R, Collilieux X, Jäggi A, Schmitz M, Dilssner F (2015) Absolute IGS antenna phase center model igs08.atx: status and potential improvements. J Geod 90(4):343–364. doi:10.1007/s00190-015-0876-3

Springer TA (2009) NAPEOS mathematical models and algorithms. Tech. Rep. DOPS-SYS-TN-0100-OPS-GN, ESA/ESOC, Darmstadt

Steigenberger P, Dach R, Prange L, Montenbruck O (2015a) Galileo satellite antenna modeling. In: Geophys Res Abstr 17, EGU2015-10772-1

Steigenberger P, Hugentobler U, Loyer S, Perosanz F, Prange L, Dach R, Uhlemann M, Gendt G, Montenbruck O (2015b) Galileo orbit and clock quality of the IGS Multi-GNSS Experiment. Adv Space Res 55(1):269–281. doi:10.1016/j.asr.2014.06.030

Steigenberger P, Montenbruck O, Hugentobler U (2015c) GIOVE-B solar radiation pressure modeling for precise orbit determination. Adv Space Res 55(5):1422–1431. doi:10.1016/j.asr.2014.12.009

Uhlemann M, Gendt G, Ramatschi M, Deng Z (2015) GFZ global multi-GNSS network and data processing results. In: Willis P (ed) IAG 150 Years. International Association of Geodesy Symposia 143. doi:10.1007/1345_2015_120

Valle P, Netti A, Zolesi M, Mizzoni R, Bandinelli M, Guidi R (2006) Efficient dual-band planar array suitable to GALILEO. In: Proceedings of the First European Conference on Antennas and Propagation (EuCAP 2006). doi:10.1109/EUCAP.2006.4584868

Wermuth M, Montenbruck O, van Helleputte T (2010) GPS high precision orbit determination software tools (GHOST). In: 4th International Conference on Astrodynamics Tools and Techniques, Madrid

Zhu SY, Massmann FH, Reigber C (2003) Satellite antenna phase center offsets and scale errors in GPS solutions. J Geod 76(11):668–672. doi:10.1007/s00190-002-0294-1